Macromolecules

pubs.acs.org/Macromolecules Article

Heterogeneous Nucleation of High-Density Polyethylene Crystals on Graphene within Microdomains

Nathan W. Volchko and Gregory C. Rutledge*

Cite This: *Macromolecules* 2023, 56, 4123−4134 Read Online

ACCESS | Metrics & More | Article Recommendations

ABSTRACT: In polymer processes, nucleating agents are often used to control the kinetics of crystallization, but their application remains largely a matter of trial and error. Thermodynamically, the efficiency of a nucleating agent can be quantified by the difference in substrate/crystal, crystal/melt, and substrate/melt interfacial energies, $\Delta\sigma$. In this work, the efficiency of graphene nanoplatelets (GNP) as nucleating agents for high-density polyethylene (HDPE) is investigated. HDPE nucleates and crystallizes rapidly, so $\Delta\sigma$ can be especially difficult to measure experimentally. To overcome this difficulty, blends of HDPE+GNP are confined to microdomains so that crystallization becomes nucleation limited. Two methods of microdomain formation are employed. In the first, HDPE+GNP is melt-blended with an immiscible matrix of polystyrene (PS), and crystallization is characterized using differential scanning calorimetry (DSC); in the second, dispersions of HDPE+GNP in toluene are sprayed onto PS substrates, and crystallization is characterized with polarized optical microscopy (POM). Heterogeneous nucleation rates at several crystallization temperatures and for several GNP loadings were measured by these two methods and found to give excellent agreement across GNP loadings. The value of $\Delta\sigma$ for HDPE+GNP is calculated to be 0.83 ± 0.18 erg/cm^2. This value is only 2.8 times larger than that reported for HDPE nucleated heterogeneously on a HDPE fiber, a nearly ideal nucleating agent for HDPE, and much smaller than many of the best nucleating agents reported for other polymers. We conclude that GNP is an efficient nucleating agent for HDPE.

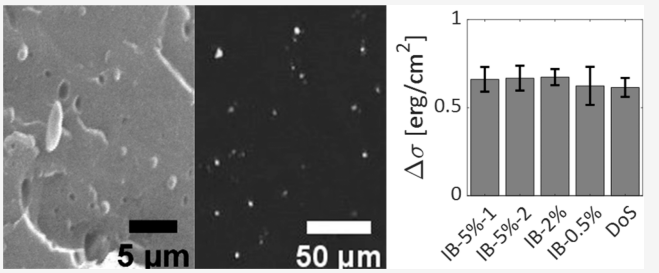

INTRODUCTION

The organization of a semicrystalline polymer into crystalline and noncrystalline domains, or its microstructure, has a large effect on the mechanical,[1−5] thermal,[6] electrical,[7,8] and optical[9−13] properties of the polymer. This microstructure depends on many factors, one of which is the kinetics of crystallization. In most cases, polymers crystallize through the processes of nucleation and growth, by which small stable crystalline clusters, called nuclei, form first, and these nuclei subsequently grow by accretion of polymer from the surrounding melt or solution. The kinetics of nucleation and growth can be manipulated by changes in temperature, pressure, flow-induced melt structure, or the introduction of nucleating agents (NA), which alter the rate of nucleus formation[14] or may promote the formation of one crystal polymorph over another.[15,16] NAs can be crystalline powders of small molecules[17−20] or other polymers.[21−24] Self-nucleation occurs on crystalline residuals from an incompletely melted polymer.[25−29] NAs thus provide a mechanism by which to tailor macroscopic properties for a desired application.[30] However, determining the "effectiveness" of a NA is still largely a matter of empiricism.[20]

The study of nucleation, and NAs, is complicated when nucleation and growth occur concurrently, as is often the case when new nuclei are forming at the same time as old nuclei are growing. Thus, a crystallization rate obtained from the measurement of a bulk kinetic property, such as the rate of release of enthalpy of crystallization, is usually influenced by both nucleation and growth. Nucleation rates are even more difficult to measure for highly effective NAs, which cause nucleation to occur so rapidly that it is often considered to be "instantaneous" relative to subsequent crystal growth.

To study nucleation alone, Vonnegut introduced the droplet method, wherein the extent of crystal growth that is allowed following a nucleation event is limited by the size of the droplet.[31] By limiting the size of droplets so that the time to nucleate is much longer than the time for a nucleated crystal to grow to the full extent of the droplet, observations like the rate of release of crystallization enthalpy are determined by nucleation. For polymers, it is important that droplets are large enough so that the polymer chains themselves can behave as in an unconfined melt,[32−35] yet small enough to ensure that

Received: February 24, 2023
Revised: April 21, 2023
Published: May 15, 2023

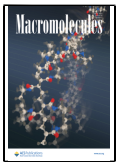

https://doi.org/10.1021/acs.macromol.3c00342
Macromolecules 2023, 56, 4123−4134

nucleation rate is dominant. Confinement on the order of hundreds of nanometers to a few micrometers in diameter has been shown to satisfy these requirements.[34]

For polymers, a variation of the droplet method involves melt-blending two immiscible polymers, such that the crystallizable polymer is the minor component of the two-phase mixture and dispersed within microdomains. Rasmussen and Loper used this type of sample for nucleation measurements with differential scanning calorimetry (DSC).[36] Santana and Müller subsequently extended this approach to the study of homogeneous nucleation of isotactic polypropylene (iPP) blended with polystyrene (PS).[37] More recently, heterogeneous nucleation of iPP blended with additives,[27] high-density polyethylene (HDPE) at the interface with iPP,[24] and self-nucleation of HDPE[29] have been investigated using microdomains in an immiscible matrix. In addition to measuring nucleation rates, the mechanisms of epitaxy (with a crystalline matrix) and graphoepitaxy due to roughness of the interface with the surrounding amorphous or crystalline matrix have been observed in these two-phase mixtures.[38] A comprehensive review of this methodology was presented very recently by Fenni et al.[38] One advantage of this method is the ability to quantify nucleation rates at multiple temperatures. Using the temperature dependence of nucleation rate and applying classical nucleation theory, the critical free energy barrier to nucleation can be calculated. This energy is a useful metric for quantifying the effectiveness of a NA.

The phenomenon of dewetting of a crystallizable polymeric melt or solution upon a substrate offers another strategy to form microdomains or droplets. In this method, a thin film of crystallizable polymer is first spin-coated as melt or solution on top of a second material (substrate) and rapidly cooled or the solvent evaporated. Upon heating above T_m, the crystallizable polymer dewets from the substrate and coalesces into droplets. Because this method produces droplets at a much lower number density relative to melt-blended samples, DSC is generally too insensitive to measure crystallization of these droplets. Instead, polarized optical microscopy (POM) can be used to track crystallization within these droplets. This method has been used to study nucleation of poly(ethylene oxide) on PS[39−42] and HDPE on PS.[43] A significant advantage of this method is that the crystallization of individual droplets can be observed directly, and the induction time correlated to the size of the crystallizing droplet. Nucleation on lines, at interfaces, or within the volumes of droplets can be distinguished by their different scalings with droplet radius.[42]

Graphene has been widely studied as a nanofiller for HDPE. HDPE−GNP composites have improved mechanical,[4,44] electrical,[44,45] thermal,[44−46] and gas barrier properties[44] relative to neat HDPE. GNP has also been shown to increase the rate of crystallization of HDPE, attributed to enhanced nucleation.[4,46,47] However, these studies are limited to bulk crystallization and only report increased crystallization temperatures, reduced crystallization half-times (or the time to reach 20% relative crystallinity in the case of Bourque et al.[4]), and fitted Avrami constants. A noteworthy exception is the work of Tarani et al.,[47] who also report apparent activation energies calculated by the Friedman method. While useful in quantifying enhanced nucleation, these apparent activation energies are not intrinsic values for the HDPE+GNP system, as they depend on GNP loading.

In this paper, we examine the heterogeneous nucleation of HDPE on GNPs within microdomains using two different methods: DSC of immiscible blends of HDPE+GNP dispersed in PS matrices and POM of HDPE+GNP droplets on a PS substrate. The nucleating efficiency of a powdered additive in HDPE as measured by these methods is reported for the first time. Estimates of the magnitude of the interfacial free energy difference (a key component of the critical free energy barrier to nucleation) are obtained and compared.

METHODS

Materials. All materials were obtained commercially from MilliporeSigma. The polyethylene was a high-density resin with a melt flow index of 12 g/10 min at 190 °C and 2.16 kg load, with a density of 0.952 g/mL as-received. The polystyrene was atactic with M_w = 192 kDa. Graphene was obtained as a powder with a nominal particle size of 5 μm.

Crystal Growth Rate. To measure the linear crystal growth rate of this HDPE, a small amount of HDPE was melted between two glass slides and pressed to form a thin film. The sample was placed in a hot stage (Linkam LTS350 hot stage, Linkam TMS 94 controller), covered with a heat shield containing a small hole for observation to minimize thermal gradients across the sample, purged with nitrogen for 10 min to provide an inert atmosphere to limit polyethylene degradation at elevated temperatures, and melted for 5 min before being quenched to the desired crystallization temperature. Isothermal crystal growth was measured between 118 and 124 °C, at 1 °C increments. The linear growth rate was obtained from the rate of change of spherulite radii as a function of time using polarized optical microscopy (POM, Zeiss Axioplan 2), with snapshots taken every 10 s (Zeiss AxioCam MRc).

Nucleation Rate. *Domains in Immiscible Blends.* For this method, the experimental design of Santana and Müller[37] and Wang et al.[27] was used. An immiscible blend of micrometer-sized domains of polyethylene and graphene nanoplatelets (HDPE+GNP) in a polystyrene (PS) matrix was prepared by first melt-blending graphene at various weight fractions (5, 2, and 0.5 wt %) with HDPE in a twin blade blender (Brabender ATR Plasticorder with a three-piece mixer) for 10 min at 180 °C and 100 rpm. This blend of HDPE+GNP was then mixed at 15 wt % in PS for 30 min at 180 °C and 100 rpm. The PS/HDPE+GNP sample was hot pressed (Carver Model C) at 115 °C (above the glass transition temperature of PS but below the melting temperature of HDPE) to a thickness of roughly 1 mm. A 3 mm disc was punched out for DSC analysis. We refer to this method as immiscible blending (IB).

Thermal characterization was performed using DSC (TA Instruments DSC 2500). A reference pan containing PS of similar mass to each sample was used to reduce the effects of the endothermic hook observed upon quenching from the melt to the crystallization temperature.[48] Between each experiment, the sample was melted at 180 °C for 2 min. The sample was then either cooled at a fixed rate (10 °C/min) for nonisothermal crystallization or quenched and held at a fixed temperature (121, 122, 123, and 124 °C) for isothermal crystallization. Crystallization was analyzed by tracking the exothermic heat flow of the sample.

Droplets on Substrate. For this method, the experimental design of Carvalho and Dalnoki-Veress[43] was followed, with some modification. Rather than spin-coating HDPE onto the desired substrate, HDPE microcrystals containing nucleating agents were sprayed from solution onto the PS substrate. This method has several advantages. First, it is widely applicable to a variety of substrates, not just those for which HDPE dewets. Second, it avoids the long equilibration times in an oven at elevated temperatures required to ensure that HDPE dewets from the substrate into microdroplets. Third, the HDPE and nucleating agents are less likely to become separated due to retraction of the three-phase contact line on the substrate, which can result in deposition of the nucleating agents on the substrate outside of the polymer droplets. We refer to this method as droplets on substrate (DoS).

First, microcrystals of HDPE containing GNP were formed in toluene via a self-seeding process. HDPE (0.1 wt %) and GNP (0.01

https://doi.org/10.1021/acs.macromol.3c00342
Macromolecules 2023, 56, 4123−4134

wt %) were sonicated in toluene for 15 min to break up the GNP from its aggregated state as received. Then, the HDPE was crystallized in solution by self-seeding, as follows: first, the solution was heated to the boiling point of toluene (110.6 °C) for 10 min to dissolve the HDPE; second, the HDPE was crystallized onto suspended GNP by cooling to 80 °C; third, the resulting dispersion was reheated until the HDPE crystals were almost completely redissolved, as confirmed visually; fourth, the solution was cooled once again to 25 °C for the self-seeded crystallization. The crystals formed during the first two steps are generally too large for the DoS method. The self-seeding step leads to HDPE+GNP particles that are smaller and more uniform in size. This solution containing HDPE microcrystals was then sprayed with an airbrush onto a spin-coated PS substrate to create the DoS sample that was used for thermal experiments. Residual toluene was removed by heating the DoS sample under an inert atmosphere.

A fully formed DoS sample was thermally characterized using a hot stage (Linkam LTS350 hot stage, Linkam TMS 94 controller) in combination with POM (Zeiss Axioplan 2, Zeiss AxioCam MRc). The sample was covered by a heat shield, and the hot stage was purged with nitrogen for 10 min and then sealed. The hot stage was heated to 160 °C for 5 min to completely melt the HDPE. The sample was then quenched and held at the desired temperature for isothermal crystallization, with snapshots taken every 10 s. Crystallization was analyzed by tracking the time when molten droplets, which appear dark when viewed through crossed polarizers, turn bright due to the formation of birefringent crystals. Compared to the large number (millions) of nucleation events that occur in a single IB experiment, a significantly smaller number of nucleation events (100 to 200) were observed per experiment by DoS; for this reason, all DoS experiments were performed in triplicate, and the results were added together.

Particle Size Distributions. The morphologies of IB samples were examined with scanning electron microscopy (SEM, SEC Co. SNE-4500 M Plus). Particle size distributions (PSD) for each sample were measured from cross sections of hot-pressed material from DSC sample preparation. Samples were cooled in liquid nitrogen for 10 min and then fractured in five places to obtain cross sections. These fractured cross sections were sputter-coated with gold and viewed at 1000× magnification with SEM under vacuum with an accelerating voltage of 30 kV.

The PSD of GNPs were measured with SEM. First, dilute suspensions of GNP in toluene (0.01 wt %) were sonicated for 15 min. Then, this suspension was drop-coated onto an SEM stage and heated on a hot plate at 50 °C to evaporate the solvent. Samples were viewed at 200× and 1000× magnification.

Particle sizes for all samples were counted using Fiji.[49] HDPE domains and GNP in microscopy images were approximated as ellipsoids. Effective diameters were calculated as the diameter of a sphere of equivalent volume for IB and DoS samples, and the diameter of a circle of equivalent area for GNPs.

RESULTS

Crystal Growth Rate. According to Lauritzen−Hoffman theory,[50,51] the crystal growth rate can be described by

$$\log G = \log G_0 - \frac{U^*}{R(T_c - T_\infty)} - \frac{K_g}{T_c \Delta T f} \quad (1)$$

where G_0 in the first term is the growth rate prefactor, which is assumed to be relatively insensitive to temperature. The second term describes the transport resistance, where U^* is the activation energy for diffusion across the interface between the crystal and melt phases, R is the universal gas constant, T_c is the crystallization temperature, and T_∞ is the temperature at which all viscous motion stops. The third term describes secondary nucleation, where K_g is the secondary nucleation constant, $\Delta T = T_m^0 - T_c$ is the degree of undercooling below the equilibrium melting temperature (T_m^0), and f is a correction, given by

$$f = \frac{2T_c}{T_c + T_m^0} \quad (2)$$

Values for material specific parameters were obtained from the literature: U^*, T_∞, and T_m^0 are 6276 J/mol,[52] 160 K,[52] and 416 K,[53,54] respectively. The crystal growth rate, log G, is plotted versus the inverse of $T_c \Delta T f$ in Figure 1. The experimental data follow Lauritzen−Hoffman theory reasonably well and are consistent with prior reports for HDPE in this temperature range.[55]

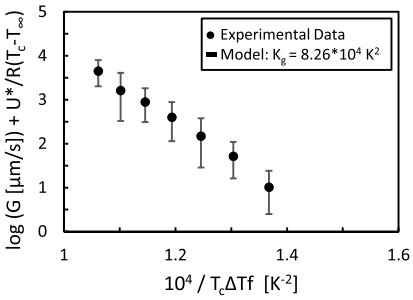

Figure 1. Experimentally measured crystal growth rate (filled circles) plotted according to Lauritzen−Hoffman theory (dotted line).

Size Distributions of IB Domains. Representative cross sections of the IB samples prepared by freeze-fracturing are shown in Figure 2. The small ellipsoidal-shaped domains in each image are HDPE+GNP. The edges of many steps are also visible where the sample did not fracture smoothly. PSDs were formed from five images for each sample, with population sizes of roughly 1000 droplets per sample. The HDPE domain sizes were well-described by log-normal distributions; the results are shown in Figure 3. Number and volume averaged diameters are provided in Table 1. With the melt blending procedure used here, HDPE+GNP domain sizes were reproducible, and no dependence of droplet size on GNP loading was observed.

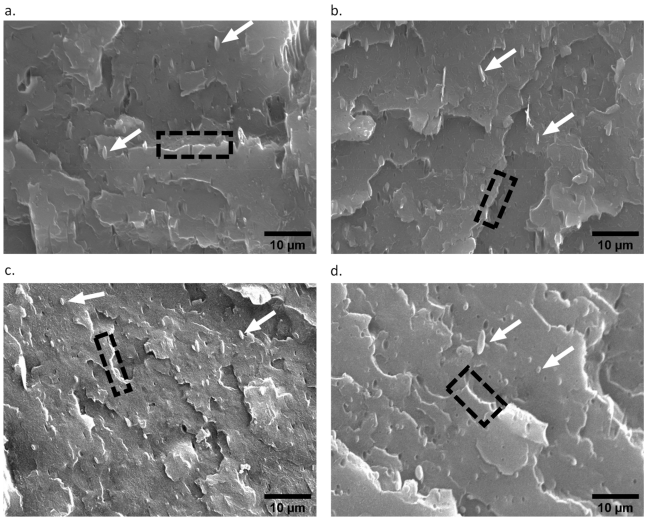

Figure 2. Cross-sectional SEM images from IB samples (% refers to GNP wt % in HDPE): (a) IB-5%-1, (b) IB-5%-2, (c) IB-2%, and (d) IB-0.5%. In each image, the white arrows highlight HDPE+GNP domains, and the dashed rectangles highlight jagged fracture planes.

https://doi.org/10.1021/acs.macromol.3c00342
Macromolecules 2023, 56, 4123−4134

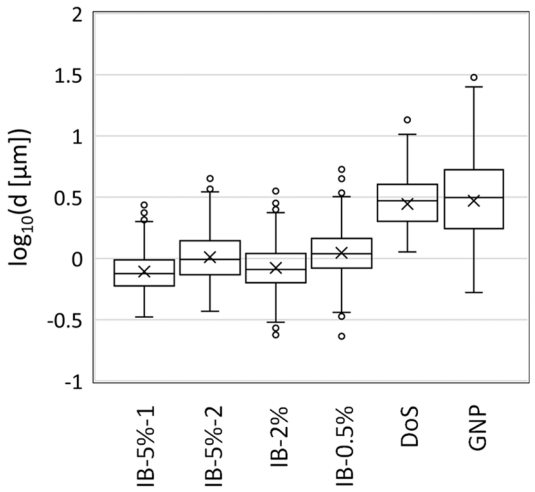

Figure 3. Box-and-whisker plots of the particle size distributions of the diameters (d) of HDPE+GNP domains in both IB and DoS samples and for GNP on its own. For each sample, the boxes indicate the 25th, 50th, and 75th percentiles; bars extending from the boxes indicate the range of the data excluding outliners; ○'s indicate outliers; ×'s indicate means.

Table 1. Characteristic Sizes of Polyethylene Domains and GNPs[a]

sample	d_n [μm]	d_v [μm]
IB-5%-1	0.84	1.43
IB-5%-2	1.13	2.09
IB-2%	0.91	1.62
IB-0.5%	1.21	2.26
DoS	3.13	
GNP	4.48	

[a] d_n and d_v are the number and volume averaged diameters, respectively.

Size Distributions of DoS Droplets. Optical images of a DoS sample are shown in Figure 4. Under crossed polars,

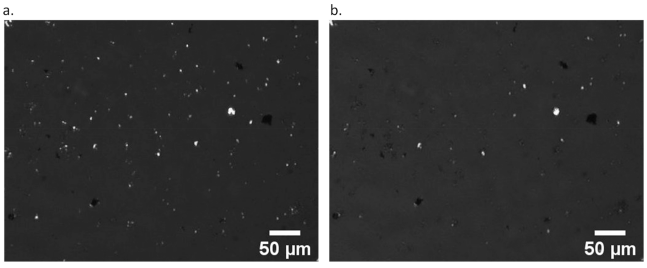

Figure 4. Polarized optical microscopy images of a DoS sample: (a) at room temperature; (b) part of the way through the crystallization procedure.

crystallized HDPE droplets appear bright, while molten droplets appear dark. Figure 4a shows the sample at room temperature, while Figure 4b shows the same sample during crystallization, after only a fraction of the droplets has nucleated and crystallized. The PSD and the number-averaged diameter of the DoS sample are included in Figure 3 and Table 1. Because nucleation events for DoS samples were determined visually, the number-average rather than volume-average particle diameter was used. The average droplet sizes were three times larger in DoS samples than IB samples.

Size Distribution of Graphene Nanoplatelets. SEM images of drop-coated GNPs are shown in Figure 5.

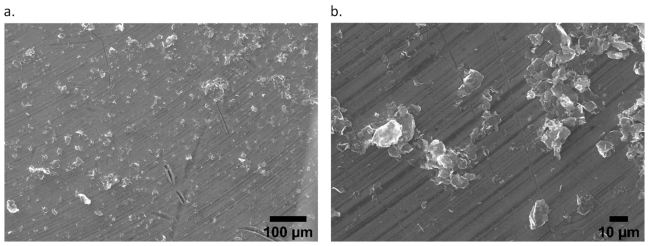

Figure 5. Characterization of GNPs. SEM image of GNPs after sonication in solvent and drop-coating on a sample holder: (a) 200× magnification; (b) 1000× magnification. For purposes of determining PSD, both magnifications were used. Because the image viewed at 1000× covers only 1/25th the area of the image at 200×, the relative frequency of data at the higher magnification was weighted by this factor before combining with the data at the lower magnification.

Aggregations of GNPs are noticeable in these images; we believe such aggregates formed while the suspension dried. Aggregates that could not be visually separated into distinct, individual platelets were not measured. To image a large number of platelets, two magnifications were used. The PSD of as-received GNPs is shown in Figure 3. The number average diameter of this PSD is included in Table 1. Of note, only 12% of the GNPs have diameters smaller than 1 μm in the as-received sample, which was subjected only to sonication before imaging; the majority of GNPs are larger than the HDPE domain sizes in the IB samples. Nevertheless, the DSC results clearly indicate the presence of GNPs within the HDPE domains (*vide infra*). It is also possible that the melt blending procedure used for IB samples alters the GNP PSD by fracturing larger platelets into smaller ones. GNPs do not experience such mechanical attrition during preparation of DoS samples; however, those droplets are larger, so that a larger fraction of the GNP population fits inside the HDPE domains of the DoS sample. For these reasons, the loadings of GNPs within HDPE microdomains of all samples are likely to be smaller than the nominal values.

Nucleation Rate. *Domains in Immiscible Blends.* To determine the temperature range where GNPs nucleate HDPE, samples were cooled from the melt at 10 °C/min. The DSC exotherms are shown in Figure 6. Also included in Figure 6 is the exotherm from a sample of PS/HDPE without GNPs. The sample without GNPs shows no crystallization until approximately 80 °C, which can be traced to heterogeneous nucleation at the interface between the HDPE and PS phases, consistent with reports in the literature for other PS/HDPE systems.[29,43] By contrast, samples containing GNP exhibit a strong exothermic peak near 120 °C, also consistent with prior reports for HDPE+GNP systems.[4,45,47] The volume fraction of droplets containing GNPs was calculated by integrating the two crystallization peaks and expressing as a fraction of the total enthalpy. In samples containing nominally 2 to 5 wt % GNP, >95% of domains nucleated on GNPs, while in samples containing nominally 0.5 wt % GNP, this fraction dropped to 83%.

From the thermograms shown in Figure 6, four temperatures were chosen for isothermal crystallization experiments (121 to 124 °C, in 1 °C increments). These temperatures were chosen to target the leading edge of the crystallization peaks in Figure

https://doi.org/10.1021/acs.macromol.3c00342
Macromolecules 2023, 56, 4123−4134

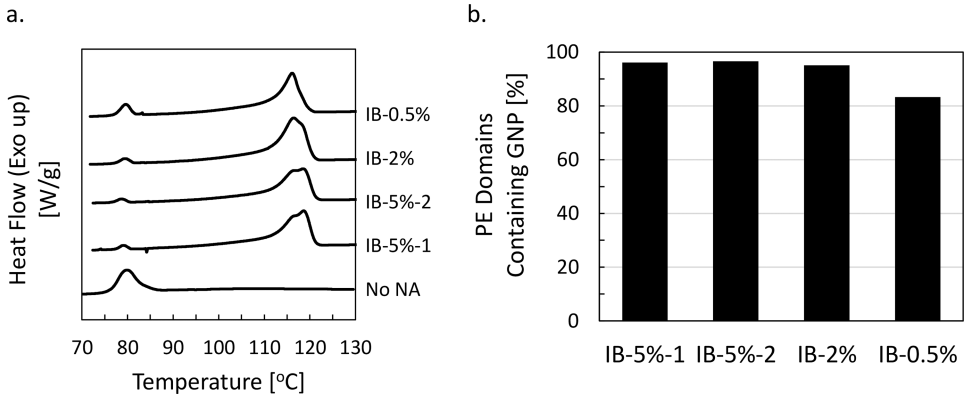

Figure 6. Crystallization of IB samples in DSC experiments with constant cooling rates from the melt. (a) DSC thermograms of all IB samples compared to a sample containing no GNP. (b) Volume fraction of PE droplets in the graphene-nucleated peak for each IB sample.

6a, where a nucleation limited process is most likely to occur. This nucleation-limited assumption is confirmed in the Discussion section.

At the lower temperatures (121 and 122 °C), HDPE+GNP nucleated so quickly that the presence of an endothermic hook during the quench to T_c masked the onset of crystallization unless care was taken to use a reference pan containing PS similar in thermal mass to the sample itself. A comparison between an empty reference pan and one containing PS is shown in Figure 7; a small overshoot is still present due to a

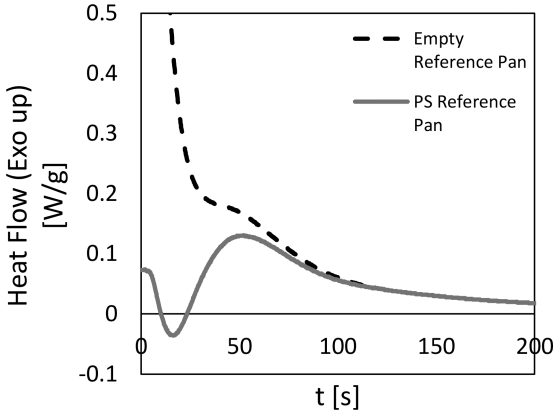

Figure 7. Isothermal crystallization exotherms using an empty reference pan (dashed black line) and using a reference pan containing polystyrene (solid gray). The black arrow indicates the presence of an endothermic hook that masks the initial onset of crystallization at short times when using an empty reference pan.

close but still imperfect matching of the thermal masses of reference and sample pans. Figure 8 shows the resulting isothermal crystallization exotherms for a representative sample (IB-5%) at each temperature. Also included in this figure is the temperature evolution of each sample during crystallization. Even at the deepest undercooling, the temperature was already within 0.6 °C of T_c at the start of crystallization. The final crystallinities achieved during isothermal crystallization experiments were calculated by integrating the area under the curves and normalizing by the specific enthalpy of fusion Δh_f = 280 J/cm^3, using a density of 1.003 g/cm^3 for the polyethylene crystal.[51,53,54,56] These values are reported in Table 2. The final crystallinities decrease with decreasing GNP loading, as expected, and with increasing T_c, which we attribute to the difficulty in growing larger nuclei at higher T_c.

The relative crystallinity by mass, w_c, was calculated as a function of time using

$$w_c = \frac{\Delta h(t)}{\Delta h_{total}} \tag{3}$$

where $\Delta h(t)$ is the specific enthalpy released as a function of time, and Δh_{total} is total specific enthalpy released by the end of the experiment. These enthalpies were calculated by integrating the heat flow curves measured by DSC in Figure 8. The relative crystallinity by volume was calculated by[57]

$$X = \frac{w_c}{w_c + \frac{\rho_c}{\rho_a}(1 - w_c)} \tag{4}$$

where ρ_c is the density of a perfect HDPE crystal (1.003 g/cm^3) and ρ_a is the density of amorphous HDPE at 25 °C (0.850 g/cm^3).[58] Figure 9 shows the evolution of relative crystallinities for the IB samples at each of the nominal GNP loadings. The curves are roughly sigmoidal in shape, and the rate of crystallization decreases with increasing temperature for each sample, as expected.

Droplets on Substrate. Three DoS samples were crystallized isothermally at each of the four temperatures employed for the IB samples. The relative crystallinity as a function of time was calculated as the number fraction of droplets crystallized with respect to the total number of droplets that crystallized at that temperature. The evolution of relative crystallinity is shown in Figure 10. While small droplets nucleated and turned bright instantaneously to the eye, crystallites in larger droplets at higher temperatures sometimes grew in size over two successive images. In such instances, the time at which light transmission was first detected in the droplet was taken as the induction time.

Avrami Model. The Avrami equation can be written as

$$\log(-\log(1 - X)) = \log K + n \log(t - t_0) \tag{5}$$

where t_0 is the induction time prior to the onset of crystallization, K is the crystallization rate, and n is the Avrami index, often presented as

$$n = n_G + n_N \tag{6}$$

where n_G is the dimensionality of growth, and n_N takes values based on the type of nucleation, with 0 corresponding to instantaneous nucleation, 1 corresponding to sporadic

https://doi.org/10.1021/acs.macromol.3c00342
Macromolecules 2023, 56, 4123−4134

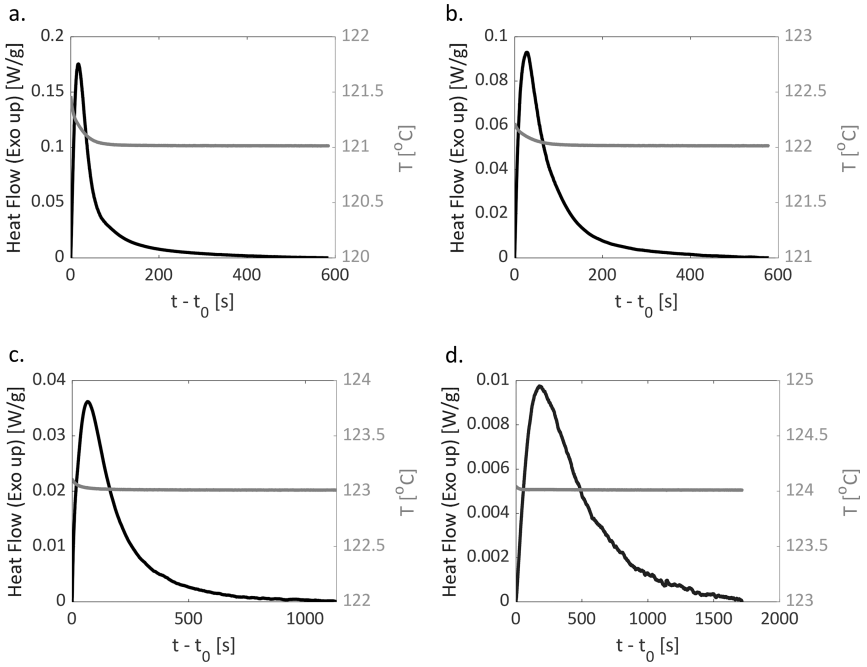

Figure 8. Isothermal crystallization data for a representative IB sample (IB-5%) at (a) 121, (b) 122, (c) 123, and (d) 124 °C. Heat flow is shown in solid black (left axis), while the temperature profile is shown in gray (right axis).

Table 2. Final Crystallinities of Each IB Sample

	crystallinity [%]			
sample	121 °C	122 °C	123 °C	124 °C
IB-5%-1	24	20	18	13
IB-5%-2	24	19	17	12
IB-2%	27	20	18	11
IB-0.5%	13	6	4	2

nucleation, and 0.5 corresponding to diffusion-limited nucleation. Noninteger values of n_N are often reported and explained as nucleation that has both sporadic and instantaneous contributions.[57]

The parameters in the Avrami equation were obtained by fitting eq 5 to data for fractional crystallinity versus time, $X(t)$, for low crystallinities, X = 0.03−0.2, where the assumptions underlying the Avrami equation are most accurate.[59] The effects of secondary crystallization processes, such as

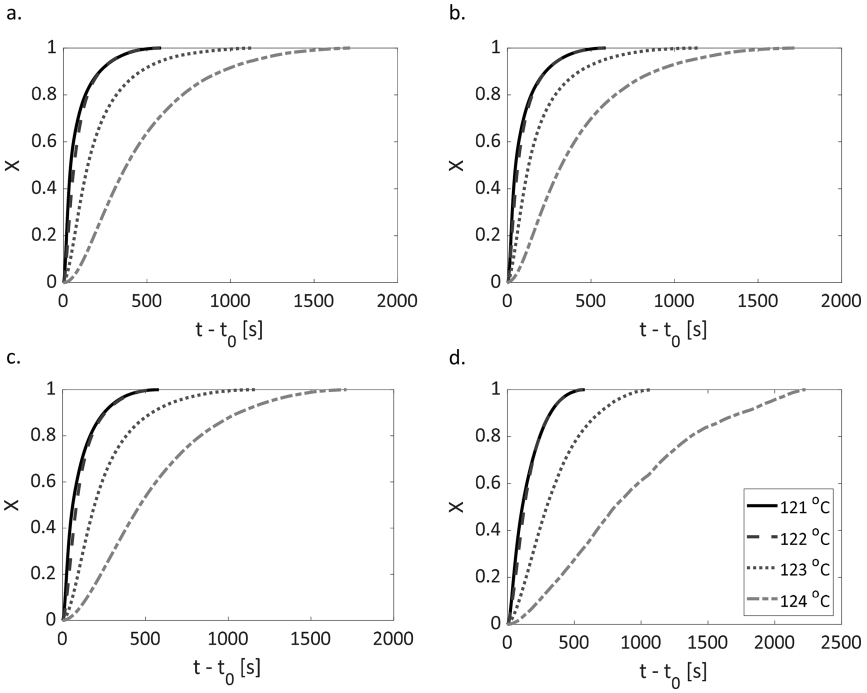

Figure 9. Relative crystallinity as a function of time for all IB isothermal crystallization experiments: (a) IB-5%-1, (b) IB-5%-2, (c) IB-2%, and (d) IB-0.5%.

https://doi.org/10.1021/acs.macromol.3c00342
Macromolecules 2023, 56, 4123−4134

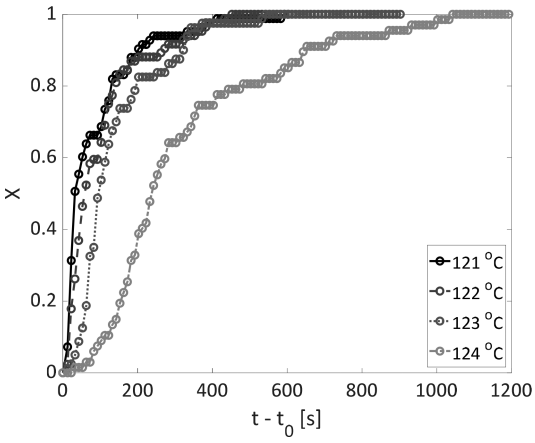

Figure 10. Crystallized fraction as a function of time for DoS isothermal crystallization experiments at each crystallization temperature. Data were combined from three experiments (~500 droplets).

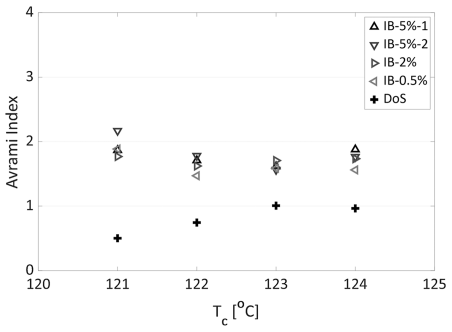

Figure 12. Avrami index as a function of crystallization temperature for the several IB and DoS conditions studied in this work.

isothermal thickening, which can be significant for HDPE, are thus minimized. A representative case showing the quality of fit is provided in Figure 11. The fitted values for the Avrami index, n, for each sample are shown in Figure 12. Within the recommended region of low conversion, IB samples generally exhibit n values between 1.5 and 2, while the averaged DoS sample has n values between 0.5 and 1. An n value near 1 is consistent with a nucleation-limited process. The larger n values exhibited by IB samples suggest that these samples may not be entirely nucleation-limited, despite the small sizes of the HDPE domains (cf. Figure 3). This observation is considered further in the Discussion section.

First-Order Nucleation Model. For a nucleation-limited process, the uncrystallized fraction of HDPE domains for both sample types should evolve in time according to

$$\log(1 - X) = -J(t - t_0) \tag{7}$$

where X is the crystallized fraction of domains and J is the nucleation rate. From classical nucleation theory,[51,60] the nucleation rate for heterogeneous nucleation is

$$\log(J) = \log(J_0) - \frac{U^*}{R(T_c - T_\infty)} - \frac{16\sigma\sigma_e\Delta\sigma T_m^{0\,2}}{kT_c(\Delta T\Delta h_f f)^2} \tag{8}$$

where J_0 is a constant prefactor that is related to the frequency of nucleation events. J_0 is relatively insensitive to temperature but is a function of the interfacial contact area between HDPE and GNP. Parameters in the second term are the same as those defined with eq 1. The third term describes the thermodynamic driving force for crystallization, where σ and σ_e are the interfacial (crystal/melt) free energies for the lateral and stem end surfaces of the HDPE crystal, T_m^0 is the equilibrium melting temperature for the perfect HDPE crystal, k is the Boltzmann constant, and Δh_f is the enthalpy of fusion per unit volume. As previously mentioned, Δh_f has been widely accepted to be 280 J/cm^3.[51,53,54,56] Several values have been reported for $\sigma\sigma_e$ and σ, depending upon the equilibrium melting temperature that is used. Values of 1380 erg^2/cm^4 and 9.6 erg/cm^2 have been reported for $\sigma\sigma_e$ and σ, respectively, using an equilibrium melting temperature of 416 K.[53,54] These values have been chosen to allow easy comparison to nucleation results reported for HDPE+polypropylene immiscible blends that also used these values.[24] For comparison, using a higher equilibrium melting temperature of 418.7 K, $\sigma\sigma_e$ and σ have been reported to be 1062 erg^2/cm^4 and 11.8 erg/cm^2, respectively.[56]

$\Delta\sigma$ is the interfacial free energy difference ($\sigma_{substrate-crystal} + \sigma_{crystal-melt} - \sigma_{substrate-melt}$) that characterizes a specific polymer−NA pair. It is of particular importance for quantifying the effectiveness of a NA: a lower value of $\Delta\sigma$ corresponds to a lower free energy barrier to nucleation, and hence the NA is more effective for that polymer. Alternatively, $\Delta\sigma$ can be nondimensionalized by the equivalent quantity for homogeneous nucleation, σ, yielding a value for the "inefficiency" of the NA between 0 (perfect heterogeneous nucleation) and 1 (homogeneous nucleation); we thus define the thermodynamic efficiency $E = 1 - \Delta\sigma/\sigma$.

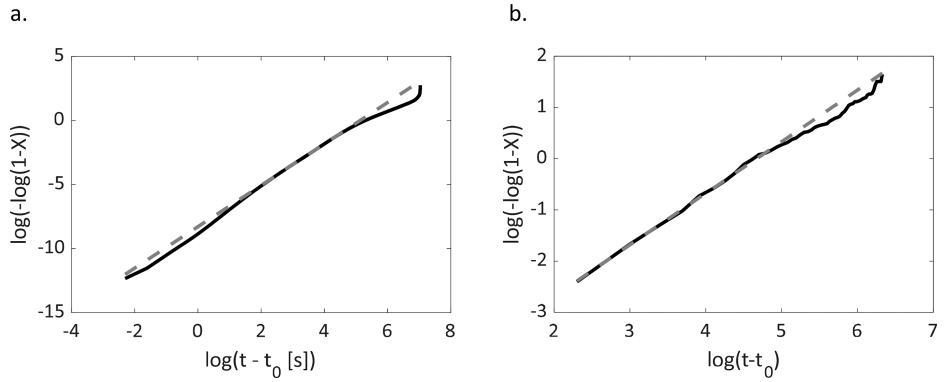

Figure 11. Representative fits of Avrami equations to the data (123 °C) for fractional crystallinity versus time: (a) IB-5%-1 and (b) DoS. Solid black lines denote experimental data, while dotted gray lines denote the Avrami model fit to 3−20% conversion.

https://doi.org/10.1021/acs.macromol.3c00342
Macromolecules 2023, 56, 4123−4134

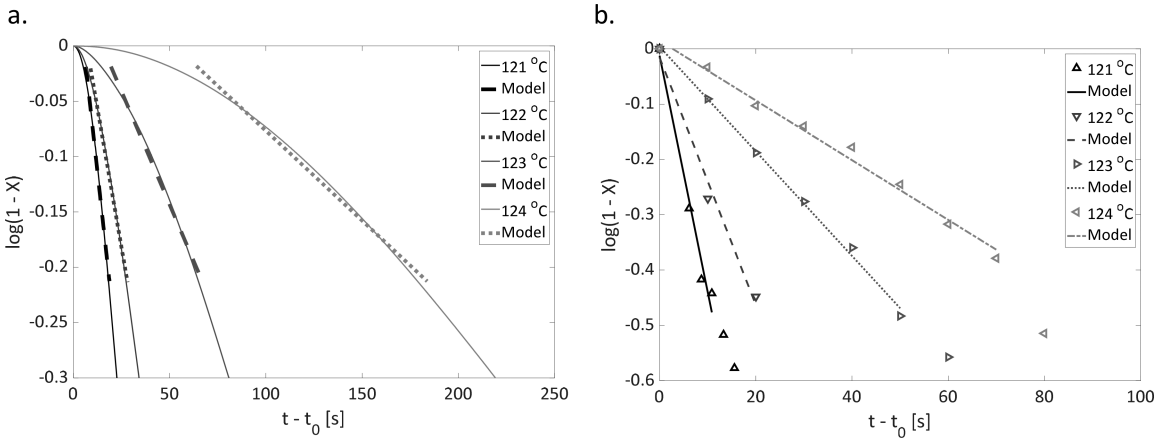

Figure 13. Examples of first-order nucleation model fit to the data for the evolution of the uncrystallized fraction of droplets: (a) IB (solid lines indicate experimental data; dotted lines indicate model) and (b) DoS (points indicate experimental data; lines indicate model).

Figure 13 shows the comparison of the best-fit first-order nucleation model to the experimental data for the four temperatures in both the IB and DoS experiments. Here also, 3−20% conversion was used to fit the nucleation model in the IB case.[24,27,57] This region was changed to 5−40% for the DoS experiment to reduce the effects of statistical noise due to the limited number of data points in the DoS experiment. For all samples, the same trend of increasing crystallization rate (steeper slope) with decreasing temperature is observed. It is clear that there is curvature in the experimental data for IB samples at higher temperature, consistent with the Avrami indices in Figure 12. In contrast, the DoS data are linear in this region.

From eq 7, the slope of the model line on a semilogarithmic plot provides an estimate of the nucleation rate between HDPE and GNP. The nucleation rate as a function of the thermal driving force is plotted in Figure 14. The nucleation rate is related to $\Delta\sigma$ and J_0 by eq 8. $\Delta\sigma$ is proportional to the slope of the best fit line through these data.

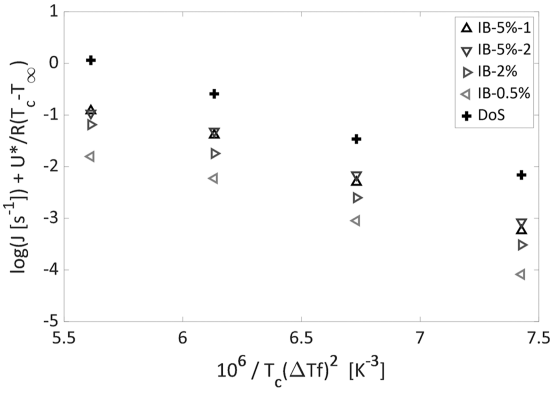

Figure 14. Nucleation rates as a function of temperature for all samples according to classical nucleation theory.

The calculated values for $\Delta\sigma$ and J_0 are shown in Figure 15. The IB and DoS experiments exhibit excellent agreement for $\Delta\sigma$. Averaging $\Delta\sigma$ over the several GNP loadings gives $\Delta\sigma$ = 0.83 ± 0.18 erg/cm^2, or an inefficiency of $\Delta\sigma/\sigma$ = 0.087 (thermodynamic efficiency E = 0.913). The value of $\Delta\sigma$ would nearly double to 1.55 erg/cm^2 and $\Delta\sigma/\sigma$ would increase by 50% using values associated with the higher T_m^0, for a thermodynamic efficiency E of 0.869. On the other hand, J_0 is roughly constant across samples. These results are discussed further in the Discussion section.

DISCUSSION

Confirmation of Nucleation-Limited Process. One of the purposes of the droplet method is to create a condition under which crystallization is nucleation-limited. For a crystallization process to be truly nucleation-limited, the induction time to observe a nucleation event ($t_{nucl} = 1/J$) must be significantly longer than the time for that crystal nucleus to grow to impingement on the edges of the droplet ($t_{grow} = (d_v/2)/G$). The ratio of t_{grow}/t_{nucl} has been named the "Turnbull number"[38] and serves as an indicator for whether the crystallization process in an IB sample is growth-dominated (Turnbull number ∼1) or nucleation-dominated (Turnbull number ≪1). From the highest nucleation rates reported in Figure 14 (DoS) and the crystal growth rates of Figure 1, the Turnbull number varies from 6 × 10^{-4} for a 1 μm domain to 3 × 10^{-3} for a 5 μm domain. Thus, for the range of domains and droplet sizes employed in this work, the induction time for nucleation is at least an order of magnitude larger than the time for subsequent growth. This is consistent with a nucleation-limited process.

Fenni et al. have discussed the significance of the Avrami index in IB samples in conjunction with the Turnbull number.[38] In self-nucleated iPP+PS IB samples, the Avrami index was indicative of a change from nucleation-controlled crystallization (n = 0.75 to 1.5, Turnbull number ≪1) to growth-controlled crystallization (n = 2 to 3.5, Turnbull number ∼1), depending upon the self-nucleation temperature that was chosen. For the present HDPE+GNP IB samples, despite very low Turnbull numbers, Avrami indices between 1.5 and 2 were calculated. Cheng et al.[46] also found Avrami indices decreased from 2.5 for neat HDPE to between 1.6 and 2.1 upon adding reduced graphene oxide (RGO) to HDPE. They attributed these values to the formation of many nuclei at the HDPE/RGO interface. These nuclei impinge upon each other at a very early stage in crystallization, forming a quasi-2D layer of spherulites and thus changing the overall dimensionality of growth. However, we observed nucleation rates that were much slower than growth. Finally, in contrast to the IB samples, the Avrami index for the DoS sample was roughly 1, as expected for nucleation-controlled crystallization. Despite

https://doi.org/10.1021/acs.macromol.3c00342
Macromolecules 2023, 56, 4123−4134

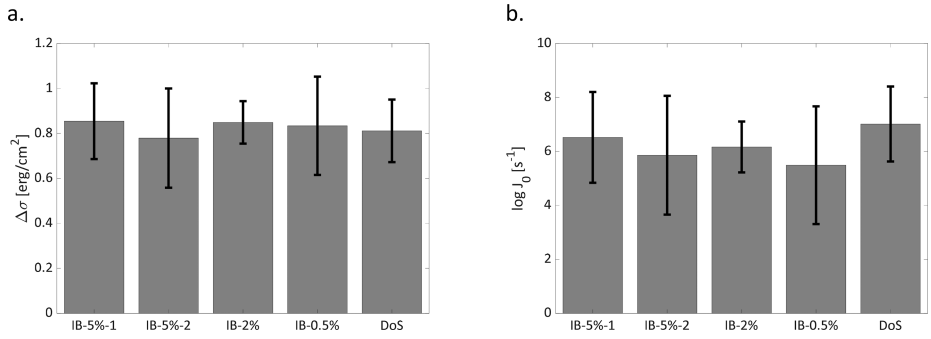

Figure 15. Fitted values of (a) interfacial free energy difference ($\Delta\sigma$) and (b) J_0. Error bars denote the 95% confidence interval for the parameter from linear regression. The averaged value for interfacial free energy difference is $\Delta\sigma = 0.83 \pm 0.18$ erg/cm^2 (95% confidence interval).

this difference, the same interfacial free energy difference, $\Delta\sigma$, was obtained from both methods, which would be inconsistent with IB samples demonstrating a growth-controlled crystallization process. The origin of the Avrami index $n > 1$ in Figure 12 must be found elsewhere.

Interfacial Free Energy Difference. From Figure 15, there is excellent agreement in the value of $\Delta\sigma$ from sample to sample and from one method to the other. Few values of $\Delta\sigma$ for HDPE heterogeneously nucleated on various substrates have been reported in the literature. Ishida and Bussi investigated heterogeneous nucleation on ultrahigh-modulus HDPE fibers.[53] Carmeli et al. used IB experiments to measure heterogeneous nucleation of HDPE at the interface with a semicrystalline iPP matrix.[24] A comparison is made in Table 3.

Table 3. Values of $\Delta\sigma$ for Various Polymer+NA Combinations and Comparison of Their Efficiencies

polymer + nucleant	$\Delta\sigma$ [erg/cm^2]	thermodynamic efficiency $E = 1 - \Delta\sigma/\sigma$
HDPE + GNP (this work)	0.826 ± 0.175	0.913
HDPE + PE fiber[53]	0.3	0.969
HDPE + iPP[24]	0.184−0.189	0.981−0.98
iPP (α) + (4,6-di-*tert*-butylphenyl)phosphate[27]	4.2	0.635 (σ from ref 61)
iPP (β) + quinacridone quinone[27]	2	0.826 (σ from ref 61)
polycaprolactone + PE fiber[62]	0.15	0.978 (σ from ref 63)
polycaprolactone + impurities[63]	1.53	0.775 (σ from ref 63)
polybutene-1 + iPP[64]	2.04	0.717 (σ from ref 65)
polybutene-1 + polybutene fiber[66]	0.31	0.957 (σ from ref 65)
poly(butylene succinate) + impurities[63]	1.97	0.841 (σ from ref 63)

For both the PE fiber and iPP, lower values of $\Delta\sigma$ were measured than our value for HDPE+GNP. This is reasonable, as both of these NAs are more similar to HDPE chemically than graphene. In fact, it is remarkable that the reported value of $\Delta\sigma$ for HDPE+iPP is smaller than that for HDPE+PE fiber. In any case, graphene has a very low barrier to nucleation. Also shown in Table 3 is a selection of data for other polymer−NA systems, highlighting the lowest values of $\Delta\sigma$ for the NAs that were reported in each case, many of which have lower thermodynamic efficiency values than the HDPE+GNP system in this work. For example, Wang et al. found that several common NAs for iPP yielded $\Delta\sigma/\sigma$ values roughly 2−4 times the value of GNP in this work yet were sufficient to act as NAs.[27] Thus, we conclude that graphene is a good nucleating agent for HDPE, a conclusion that has been reported elsewhere based on crystallization half-times, shifts in crystallization temperature, or other indirect methods.[4,46,47]

Effect of Graphene Concentration. The nucleation rates (in events/s) in Figure 14 and eq 7 do not account explicitly for the interfacial area between HDPE and GNP in each case. However, the inherent nucleation rate (in events/cm^2/s) should be independent of GNP loading. By scaling the values for J_0 relative to that for the smallest GNP loading (IB-0.5%), we can obtain an estimate of the relative interfacial area between GNP and HDPE, for comparison across all samples. Figure 14 suggests that J_0 should be proportional to GNP loading, yet this correlation is not visible in Figure 15b. Because the logarithm of J_0 appears in Eq. 8, small errors in $\Delta\sigma$ between samples lead to large errors in J_0. Thus, for this calculation, the averaged value of $\Delta\sigma$ was used to recalculate J_0 for all the samples so that a more consistent comparison could be made. The scaled interfacial areas for each sample are shown in Figure 16 (where IB-0.5% = 1). The scaled areas for

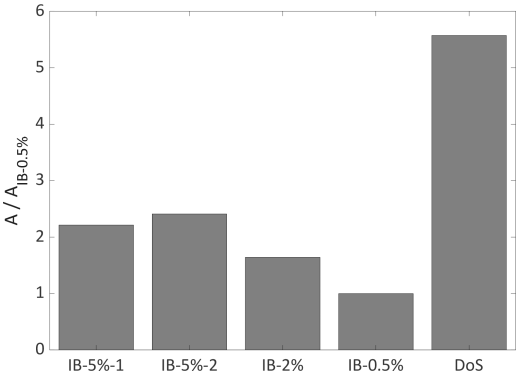

Figure 16. Interfacial contact area, A, scaled by the minimum calculated A value (IB-0.5%).

the IB-5% samples are 2.3, despite nominally an order of magnitude increase in loading; the scaled area for IB-2% is 1.6, for a nominal increase in loading by a factor of 4. Because the domain sizes are insensitive to loading, the likely explanation is an increase in the number of GNPs per domain for the nominally higher loadings. The lack of a linear relationship between nominal GNP loading and interfacial area is consistent with increased aggregation of the GNPs or exclusion of the larger GNPs from the HDPE domains. In addition, Bartczak et al. have reported the migration of impurities from the minor phase to the major phase in blends of iPP dispersed in PS;[67] this mechanism has also been noted by Fenni et al. as

https://doi.org/10.1021/acs.macromol.3c00342
Macromolecules 2023, 56, 4123−4134

a possible consequence of the melt blending procedure.[38] Given the similar nature of aromatic groups in graphene and polystyrene, it is another possibility here. In contrast, the scaled interfacial area for the DoS sample is 5.6; this result seems to support either the exclusion or migration hypothesis.

CONCLUSIONS

Droplet methods are an effective way to study stochastic processes like nucleation within a single experiment. Herein, two strategies to measure heterogeneous nucleation in microdomains of HDPE were implemented: the first strategy involving blending of HDPE+GNP within an immiscible polystyrene matrix to create isolated domains (IB) and the second involving spraying of HDPE+GNP dispersions in toluene onto a PS substrate (DoS). To the best of our knowledge, this is the first time that heterogeneous nucleation of HDPE by a powdered additive has been quantified using these two methods. In both cases, the effect of GNP on HDPE nucleation was evidenced by an increase in the temperature of crystallization by 40 °C relative to HDPE without GNPs. To study nucleation at isothermal crystallization temperatures, IB samples were characterized by DSC and DoS samples by POM. For DSC, reducing the endothermic hook during quenching was critical to measuring nucleation in fast-crystallizing HDPE.

Nucleation rates were calculated for both methods, and the effectiveness of GNP as a nucleating agent for HDPE, as characterized by the difference in interfacial energies, $\Delta\sigma$, was quantified. Excellent agreement between the two methods in the determination of this quantity was found. Finally, the magnitude of $\Delta\sigma$ for HDPE nucleating on GNP was compared to other nucleants for HDPE that have been recently published in the literature. The $\Delta\sigma$ measured in this work for GNP was only slightly larger than for HDPE nucleating at iPP interfaces[24] and at the interface with an HDPE fiber,[53] both of which are nearly ideal nucleants for HDPE. This indicates that GNP is a very effective nucleating agent for HDPE. The thermodynamic efficiency of heterogeneous nucleation, E, allows comparison across other polymer−NA systems. The high value calculated here indicates that GNP is an efficient nucleating agent for HDPE when compared to different heterogeneously nucleated polymers.

AUTHOR INFORMATION

Corresponding Author

Gregory C. Rutledge − *Department of Chemical Engineering, Massachusetts Institute of Technology, Cambridge, Massachusetts 02139, United States;* orcid.org/0000-0001-8137-1732; Email: rutledge@mit.edu

Author

Nathan W. Volchko − *Department of Chemical Engineering, Massachusetts Institute of Technology, Cambridge, Massachusetts 02139, United States*

Complete contact information is available at: https://pubs.acs.org/10.1021/acs.macromol.3c00342

Notes

The authors declare no competing financial interest.

ACKNOWLEDGMENTS

Financial support for this work was provided by the Designing Materials to Revolutionize and Engineer our Future (DMREF) and Grant Opportunities for Academic Liaison with Industry (GOALI) programs of the National Science Foundation, Division of Civil, Mechanical and Manufacturing Innovation, Award #1729304. This work made use of the Institute for Soldier Nanotechnologies Shared Experimental Facilities at MIT.

REFERENCES

(1) Callear, J. E.; Shortall, J. B. The Effect of Microstructure and Crystallinity on the Tensile Properties and Fracture Behaviour of Injection-Moulded Polytetramethylene Terephthalate. *J. Mater. Sci.* **1977**, *12*, 141−152.

(2) Clark, E. J. Molecular and Microstructural Factors Affecting Mechanical Properties of Polymeric Cover Plate Materials. *U. S. Dept. of Commerce, National Bureau of Standards* **1985**, NBSIR 85-3197.

(3) Bedoui, F.; Diani, J.; Bédoui, F.; Diani, J.; Régnier, G. Relationship between Microstructure and Elastic Properties of Semi-Crystalline Polymers. *Mater. Res. Soc. Symp. Proc.* **2005**, *882*, DOI: 10.1557/PROC-882-EE7.9.

(4) Bourque, A. J.; Locker, C. R.; Tsou, A. H.; Vadlamudi, M. Nucleation and Mechanical Enhancements in Polyethylene-Graphene Nanoplate Composites. *Polymer* **2016**, *99*, 263−272.

(5) Park, J. H.; Rutledge, G. C. Ultrafine High Performance Polyethylene Fibers. *J. Mater. Sci.* **2018**, *53* (4), 3049−3063.

(6) Selezneva, E.; di Pietro, R.; Jiao, X.; McNeill, C. R.; Sirringhaus, H. Investigation of the Effect of Microstructural Changes on Thermal Transport in Semicrystalline Polymer Semiconductors. *APL Mater.* **2019**, *7* (8), 081118.

(7) Friler, J.; Cebe, P. Effects of Crystallinity on Electrical Properties and Structure of Semicrystalline Polyimides. *Mater. Res. Soc. Symp. Proc.* **1990**, *214*, 101−106.

(8) Li, D.; Zhou, L.; Wang, X.; He, L.; Yang, X. Effect of Crystallinity of Polyethylene with Different Densities on Breakdown Strength and Conductance Property. *Materials* **2019**, *12* (11), 1746.

(9) de Santis, F.; Pantani, R. Optical Properties of Polypropylene upon Recycling. *Scientific World Journal* **2013**, *2013*, 1.

(10) Botiz, I.; Stingelin, N. Influence of Molecular Conformations and Microstructure on the Optoelectronic Properties of Conjugated Polymers. *Materials* **2014**, *7*, 2273−2300.

(11) Shen, L.; Nickmans, K.; Severn, J.; Bastiaansen, C. W. M. Improving the Transparency of Ultra-Drawn Melt-Crystallized Polyethylenes: Toward High-Modulus/High-Strength Window Application. *ACS Appl. Mater. Interfaces* **2016**, *8* (27), 17549−17554.

(12) Boztepe, S.; Gilblas, R.; de Almeida, O.; Gerlach, C.; Le Maoult, Y.; Schmidt, F. The Role of Microcrystalline Structure on Optical Scattering Characteristics of Semi-Crystalline Thermoplastics and the Accuracy of Numerical Input for IR-Heating Modeling. *Int. J. of Mater. Forming* **2018**, *11* (5), 717−727.

(13) Lin, Y.; Bilotti, E.; Bastiaansen, C. W. M.; Peijs, T. Transparent Semi-Crystalline Polymeric Materials and Their Nanocomposites: A Review. *Polym. Eng. Sci.* **2020**, *60*, 2351−2376.

(14) Wypych, G. *Handbook of Nucleating Agents*; ChemTec Publishing: Toronto, 2016.

(15) Menyhárd, A.; Molnár, J.; Horváth, Z.; Horváth, F.; Cavallo, D.; Polyák, P. Self-Organization of Micro Reinforcements and the Rules of Crystal Formation in Polypropylene Nucleated by Non-Selective Nucleating Agents with Dual Nucleating Ability. *Polym. Cryst.* **2020**, DOI: 10.1002/pcr2.10136.

(16) Jia, W.; Zhuo, R.; Xu, M.; Lin, J.; Li, X.; Liu, C.; Shen, C.; Shao, C. Synergistic Effect of Pressurization Rate and β-Form Nucleating Agent on the Multi-Phase Crystallization of iPP. *Polymers* **2021**, *13* (17), 2984.

(17) Binsbergen, F.L. Heterogeneous Nucleation in the Crystallization of Polyolefins: Part 1. Chemical and Physical Nature of Nucleating Agents. *Polymer* **1970**, *11* (5), 253−267.
(18) Wittmann, J. C.; Lotz, B. Epitaxial Crystallization of Polyethylene on Organic Substrates: A Reappraisal of the Mode of Action of Selected Nucleating Agents. *J. Polym. Sci., Polym. Phys. Ed.* **1981**, *19*, 1837−1851.
(19) Wittmann, J. C.; Hodge, A. M.; Lotz, B. Epitaxial Crystallization of Polymers onto Benzoic Acid: Polyethylene and Paraffins, Aliphatic Polyesters, and Polyamides. *J. Polym. Sci., Polym. Phys. Ed.* **1983**, *21*, 2495−2509.
(20) Seven, K. M.; Cogen, J. M.; Gilchrist, J. F. Nucleating Agents for High-Density Polyethylene - A Review. *Polym. Eng. Sci.* **2016**, *56* (5), 541−554.
(21) Bartczak, Z.; Galeski, A.; Pracella, M. Spherulite Nucleation in Blends of Isotactic Polypropylene with High-Density Polyethylene. *Polymer* **1986**, *27*, 537−543.
(22) Yan, S.; Petermann, J.; Yang, D. Epitaxial Behavior of HDPE on the Boundary of Highly Oriented iPP Substrates. *Colloid Polym. Sci.* **1995**, *273*, 842−847.
(23) Song, S.; Wu, P.; Ye, M.; Feng, J.; Yang, Y. Effect of Small Amount of Ultra High Molecular Weight Component on the Crystallization Behaviors of Bimodal High Density Polyethylene. *Polymer* **2008**, *49* (12), 2964−2973.
(24) Carmeli, E.; Fenni, S. E.; Caputo, M. R.; Müller, A. J.; Tranchida, D.; Cavallo, D. Surface Nucleation of Dispersed Polyethylene Droplets in Immiscible Blends Revealed by Polypropylene Matrix Self-Nucleation. *Macromolecules* **2021**, *54* (19), 9100−9112.
(25) Xu, J.; Ma, Y.; Hu, W.; Rehahn, M.; Reiter, G. Cloning Polymer Single Crystals through Self-Seeding. *Nat. Mater.* **2009**, *8* (4), 348−353.
(26) Michell, R. M.; Mugica, A.; Zubitur, M.; Muller, A. J. Self-Nucleation of Crystalline Phases within Homopolymers, Polymer Blends, Copolymers, and Nanocomposites. *Adv. Polym. Sci.* **2015**, *276*, 215−256.
(27) Wang, B.; Utzeri, R.; Castellano, M.; Stagnaro, P.; Müller, A. J.; Cavallo, D. Heterogeneous Nucleation and Self-Nucleation of Isotactic Polypropylene Microdroplets in Immiscible Blends: From Nucleation to Growth-Dominated Crystallization. *Macromolecules* **2020**, *53* (14), 5980−5991.
(28) Sangroniz, L.; Cavallo, D.; Müller, A. J. Self-Nucleation Effects on Polymer Crystallization. *Macromolecules* **2020**, *53*, 4581−4604.
(29) Fenni, S. E.; Caputo, M. R.; Müller, A. J.; Cavallo, D. Surface Roughness Enhances Self-Nucleation of High-Density Polyethylene Droplets Dispersed within Immiscible Blends. *Macromolecules* **2022**, *55* (4), 1412−1423.
(30) Aksel, S. Nucleation and Clarification of Polyethylenes. PhD Thesis, ETH Zurich, 2015.
(31) Vonnegut, B. Variation with Temperature of the Nucleation Rate of Supercooled Liquid Tin and Water Drops. *J. Colloid Sci.* **1948**, *3* (6), 563−569.
(32) Jin, Y.; Rogunova, M.; Hiltner, A.; Baer, E.; Nowacki, R.; Galeski, A.; Piorkowska, E. Structure of Polypropylene Crystallized in Confined Nanolayers. *J. Polym. Sci. B Polym. Phys.* **2004**, *42* (18), 3380−3396.
(33) Kailas, L.; Vasilev, C.; Audinot, J.-N.; Migeon, H.-N.; Hobbs, J. K. A Real-Time Study of Homogeneous Nucleation, Growth, and Phase Transformations in Nanodroplets of Low Molecular Weight Isotactic Polypropylene Using AFM. *Macromolecules* **2007**, *40* (20), 7223−7230.
(34) Michell, R. M.; Blaszczyk-Lezak, I.; Mijangos, C.; Müller, A. J. Confinement Effects on Polymer Crystallization: From Droplets to Alumina Nanopores. *Polymer.* **2013**, *54*, 4059−4077.
(35) Zhang, G.; Lee, P. C.; Jenkins, S.; Dooley, J.; Baer, E. The Effect of Confined Crystallization on High-Density Poly(Ethylene) Lamellar Morphology. *Polymer* **2014**, *55* (2), 663−672.
(36) Rasmussen, D. H.; Loper, C. R., Jr. DSC: A Rapid Method for Isothermal Nucleation Rate Measurement. *Acta Metall.* **1976**, *24* (2), 117−123.
(37) Santana, O. O.; Müller, A. J. Homogeneous Nucleation of the Dispersed Crystallisable Component of Immiscible Polymer Blends. *Polym. Bull.* **1994**, *32*, 471−477.
(38) Fenni, S. E.; Müller, A. J.; Cavallo, D. Understanding polymer nucleation by studying droplets crystallization in immiscible polymer blends. *Polymer* **2023**, *264*, 125514.
(39) Massa, M. V.; Carvalho, J. L.; Dalnoki-Veress, K. Direct Visualisation of Homogeneous and Heterogeneous Crystallisation in an Ensemble of Confined Domains of Poly(Ethylene Oxide). *Eur. Phys. J. E* **2003**, *12*, 111−117.
(40) Massa, M. V.; Dalnoki-Veress, K. Homogeneous Crystallization of Poly(Ethylene Oxide) Confined to Droplets: The Dependence of the Crystal Nucleation Rate on Length Scale and Temperature. *Phys. Rev. Lett.* **2004**, *92* (25), 255509.
(41) Massa, M. V.; Carvalho, J. L.; Dalnoki-Veress, K. Confinement Effects in Polymer Crystal Nucleation from the Bulk to Few-Chain Systems. *Phys. Rev. Lett.* **2006**, *97* (24), 247802.
(42) Carvalho, J. L.; Dalnoki-Veress, K. Homogeneous Bulk, Surface, and Edge Nucleation in Crystalline Nanodroplets. *Phys. Rev. Lett.* **2010**, *105* (23), 237801.
(43) Carvalho, J. L.; Dalnoki-Veress, K. Surface Nucleation in the Crystallisation of Polyethylene Droplets. *Eur. Phys. J. E* **2011**, DOI: 10.1140/epje/i2011-11006-y.
(44) López-González, M.; Flores, A.; Marra, F.; Ellis, G.; Gómez-Fatou, M.; Salavagione, H. J. Graphene and Polyethylene: A Strong Combination towards Multifunctional Nanocomposites. *Polymers* **2020**, *12* (9), 2094.
(45) Jiang, X.; Drzal, L. T. Multifunctional High-Density Polyethylene Nanocomposites Produced by Incorporation of Exfoliated Graphene Nanoplatelets 2: Crystallization, Thermal and Electrical Properties. *Polym. Compos.* **2012**, *33* (4), 636−642.
(46) Cheng, S.; Chen, X.; Hsuan, Y. G.; Li, C. Y. Reduced Graphene Oxide-Induced Polyethylene Crystallization in Solution and Nanocomposites. *Macromolecules* **2012**, *45* (2), 993−1000.
(47) Tarani, E.; Papageorgiou, D. G.; Valles, C.; Wurm, A.; Terzopoulou, Z.; Bikiaris, D. N.; Schick, C.; Chrissafis, K.; Vourlias, G. Insights into Crystallization and Melting of High Density Polyethylene/Graphene Nanocomposites Studied by Fast Scanning Calorimetry. *Polym. Test.* **2018**, *67*, 349−358.
(48) Thomas, L. C. Interpreting Unexpected Events and Transitions in DSC Results. TA Instruments TA039.
(49) Schindelin, J.; Arganda-Carreras, I.; Frise, E.; Kaynig, V.; Longair, M.; Pietzsch, T.; Preibisch, S.; Rueden, C.; Saalfeld, S.; Schmid, B.; Tinevez, J. Y.; White, D. J.; Hartenstein, V.; Eliceiri, K.; Tomancak, P.; Cardona, A. Fiji: An Open-Source Platform for Biological-Image Analysis. *Nat. Meth.* **2012**, *9* (7), 676−682.
(50) Lauritzen, J. I.; Hoffman, J. D. Extension of Theory of Growth of Chain-Folded Polymer Crystals to Large Undercoolings. *J. Appl. Phys.* **1973**, *44* (10), 4340−4352.
(51) Hoffman, J. D.; Davis, G. T.; Lauritzen, J. I. The Rate of Crystallization of Linear Polymers with Chain Folding. In *Treatise on Solid State Chemistry*; Springer: Boston, MA, 1976; Vol. 3, pp 497−614.
(52) Supaphol, P.; Spruiell, J. E. Nonisothermal Bulk Crystallization Studies of High Density Polyethylene Using Light Depolarizing Microscopy. *J. Polym. Sci. B Polym. Phys.* **1998**, *36* (4), 681−692.
(53) Ishida, H.; Bussi, P. Surface-Induced Crystallization in Ultrahigh-Modulus Polyethylene Fiber Reinforced Polyethylene Composites. *Macromolecules* **1991**, *24*, 3569−3577.
(54) Gornick, F.; Hoffman, J. D. Nucleation in Polymers. *Ind. Eng. Chem.* **1966**, *58* (2), 41−53.
(55) Lindenmeyer, P. H.; Holland, V. F. Relationship between Molecular Weight, Radial-Growth Rate, and the Width of the Extinction Bands in Polyethylene Spherulites. *J. Appl. Phys.* **1964**, *35* (1), 55−58.

https://doi.org/10.1021/acs.macromol.3c00342
Macromolecules 2023, 56, 4123−4134

(56) Hoffman, J. D.; Miller, R. L. Kinetics of Crystallization from the Melt and Chain Folding in Polyethylene Fractions Revisited: Theory and Experiment. *Polymer* **1997**, *38* (13), 3151−3212.
(57) Lorenzo, A. T.; Arnal, M. L.; Albuerne, J.; Müller, A. J. DSC Isothermal Polymer Crystallization Kinetics Measurements and the Use of the Avrami Equation to Fit the Data: Guidelines to Avoid Common Problems. *Polym. Test.* **2007**, *26* (2), 222−231.
(58) Shirazi, M. M. H.; Khajouei-Nezhad, M.; Zebarjad, S. M.; Ebrahimi, R. Evolution of the Crystalline and Amorphous Phases of High-Density Polyethylene Subjected to Equal-Channel Angular Pressing. *Polym. Bull.* **2020**, *77* (4), 1681−1694.
(59) Sperling, L. H. *Introduction to Physical Polymer Science*, 4th ed.; Wiley: 2005.
(60) Wunderlich, B. *Macromolecular Physics*; Academic Press: 1976; Vol. *2*.
(61) Clark, E. J.; Hoffman, J. D. Regime III Crystallization in Polypropylene. *Macromolecules* **1984**, *17* (4), 878−885.
(62) Ishida, H.; Bussi, P. Induction Time Approach to Surface Induced Crystallization in Polyethylene/Poly (ε-Caprolactone) Melt. *J. Mater. Sci.* **1991**, *26*, 6373−6382.
(63) Safari, M.; Mugica, A.; Zubitur, M.; de Ilarduya, A. M.; Muñoz-Guerra, S.; Müller, A. J. Controlling the Isothermal Crystallization of Isodimorphic PBS-*ran*-PCL Random Copolymers by Varying Composition and Supercooling. *Polymers* **2020**, *12* (1), 17.
(64) Chatterjee, A. M.; Price, F. P.; Newman, S. Heterogeneous Nucleation of Crystallization of High Polymers from the Melt. III. Nucleation Kinetics and Interfacial Energies. *J. Polym. Sci., Polym. Phys. Ed.* **1975**, *13*, 2391−2400.
(65) Powers, J.; Hoffman, J. D.; Weeks, J. J.; Quinn, F. A., Jr. Crystallization Kinetics and Polymorphic Transformations in Polybutene-l. *J. Res. of Natl. Bur. of Stand. - A. Phys. and Chem.* **1965**, *69A* (4), 335−345.
(66) Wang, W.; Wang, B.; Tercjak, A.; Müller, A. J.; Ma, Z.; Cavallo, D. Origin of Transcrystallinity and Nucleation Kinetics in Polybutene-1/Fiber Composites. *Macromolecules* **2020**, *53* (20), 8940−8950.
(67) Bartczak, Z.; Galeski, A.; Krasnikova, N. P. Primary Nucleation and Spherulite Growth Rate in Isotactic Polypropylene-Polystyrene Blends. *Polymer* **1987**, *28*, 1627−1634.

■ NOTE ADDED AFTER ASAP PUBLICATION

Due to a production error, this paper was published ASAP on May 15, 2023, with errors in Figures 12 and 14. The corrected version was reposted on May 19, 2023.

https://doi.org/10.1021/acs.macromol.3c00342
Macromolecules 2023, 56, 4123−4134